AJVR

AVMA

Radiological features of arterial channels in the equine third phalanx measured using a novel customized software represent changes of laminitis

Valentina Reiser, Vet Med[1]; Andreas Reiser, Dr Ing[1]; Theresia F. Licka, Dr Vet Med, DACVSMR[1,2]*

[1]Clinic for Horses, Department for Horses and Small Animals, Vienna University of Veterinary Medicine, Vienna, Austria
[2]Department of Veterinary Clinical Studies, Royal (Dick) School of Veterinary Studies, University of Edinburgh, Roslin Midlothian, Scotland

*Corresponding author: Dr. Licka (theresia.licka@vetmeduni.ac.at)

Received July 6, 2023
Accepted October 17, 2023

doi.org/10.2460/ajvr.23.07.0150

OBJECTIVE
To identify and measure radiolucencies at the solear margin of the distal phalanx in radiographs of healthy and laminitic hooves.

SAMPLE
Clinical records and dorsoproximal-palmarodistal radiographs of equine forelimbs with radiological diagnoses of either laminitis (n = 40, L) or navicular syndrome (n = 40, NS).

METHODS
Outlines of the radiolucent structures at the solar margin were drawn in ImageJ, and a customized novel plugin "Arteries Analyzer/ImageJ" was used for measurements. The diverging radiolucencies outside the terminal arc of the distal phalanx were differentiated as arterial channels (open at the solear margin) and ellipses (closed at the solear margin). Comparisons between L and NS, between distal phalanges with and without ellipses, and of arterial channels and ellipses in areas were compared using Wilcoxon and the Mann-Whitney *U* tests, respectively. The reliability and repeatability of the method were tested using Friedman's test.

RESULTS
Fewer arterial channels but more ellipses were identified in L than in NS. In phalanges with ellipses (n = 47), the number of ellipses and the number of arterial channels were negatively correlated (PCC −0.181, $P = .224$). The number of ellipses correlated positively with the severity of laminitis (PCC 0.495, $P < .001$; n = 80) and with the degree of rotation of the distal phalanx (PCC 0.392, $P < .001$; n = 80).

CLINICAL RELEVANCE
The software tool successfully measured arterial channels and ellipses outlined by the evaluators. Results indicate that healthy arteries develop into pathological ellipses in laminitic feet. This may be used to complement the interpretation of radiographs and support clinical decision-making.

Keywords: laminitis, distal phalanx, ImageJ, equine, radiology

Laminitis is a crippling disease of mechanical failure of the laminar tissue, an interdigitating fibrous structure, which suspends the distal phalanx within the hoof capsule. This failure results in rotation and sinking of the distal phalanx causing acute pain. Laminitis can result in a life-threatening debilitation for the horse[1–3] and it has a complex and multifactorial aetiology of metabolic, inflammatory, traumatic, or vascular origin.[4–6]

The initial or developmental phase of laminitis can be described as a vascular disease with hypoperfusion of the digit leading to laminar ischemia with subsequent failure of the suspension of the distal phalanx.[7–9] The process of destruction of the lamellar attachment begins before the first clinical signs of laminitis are apparent.[10] The acute phase of laminitis lasts from the onset of clinical foot pain to the time when there is evidence of displacement of

the distal phalanx within the hoof capsule on clinical and/or radiological assessment. Native radiography allows for the assessment of the hoof capsule and its integrity as well as the quantification of the distal phalanx displacement and lysis on its own. Still, it provides little direct information about the digital vasculature and the surrounding of the vessels of the distal phalanx. Radiographs are indicated in every suspected laminitic case because they provide valuable information about the presence, severity, relative chronicity, and progressive nature of the disease.[11] Lateromedial radiographs have long been considered essential in the evaluation of acute and chronic laminitis; however, they only allow assessment in 1 plane.[12] Since an increasing number of distinct pathological changes are known to be associated with laminitis, including so-called capsular rotation, phalangeal rotation, distal displacement of the distal phalanx, and combined rotation and displacement events,[11] additional views to the lateromedial gold standard should be considered to document these pathological changes. Imaging evaluation of the vasculature of the hoof in different phases of laminitis has previously been done using arteriograms,[13] venograms,[14] magnetic resonance,[15] sonography imaging,[16] and scintigraphy.[17] In chronic laminitis, the vascular anatomy of the palmar digital arteries and its major branches in the equine foot were arteriographically evaluated, and fewer branches were identified than in healthy feet.[18] These studies[13,18] show that the importance of arterial vasculature for the pathogenesis and pathophysiology of laminitis is indisputable.

Nevertheless, radiographic characteristics of the bone surrounding of the arteries in the distal phalanx have not been described. The purpose of this study was to identify and describe arterial channels within the dorsal half of the distal phalanx, and to create a software tool that complements the interpretation of radiographs taken in cases of equine laminitis, supporting clinical decision-making.

Methods

Sample size

Power calculation was based on differences in blood flow of the lateral digital arteries as determined by Doppler ultrasound in cases of laminitis with radiographic changes and in healthy horses (151 ± 49 mL/min and 88 ± 17 mL/min, respectively).[19] Using suitable software (https://clincalc.com/stats/samplesize.aspx), we identified a minimum number of 21 radiographs per group as a minimum to reach a significance of $P < .01$ with a power of 95%.

Horses

The study involved clinical case notes and sets of radiographs from 2018 to 2022 of 100 horses sourced from the patient management and documentation software of the Equine Clinic, University of Veterinary Medicine Vienna. Inclusion criteria were: horse age 4 years or older; radiology report including either the diagnosis "laminitis" (L) or the diagnoses "navicular syndrome" (NS), "navicular disease," or "Podotrochleosis." Only radiographs of feet were used in the NS group where the radiological report and the clinical case notes did not include any mention of laminitis—neither in the history of the horse, nor in the request, nor in the findings of the radiological evaluations and measurements. Out of the list of 100 patient case notes that met these criteria, a group of 40 horses had a radiological diagnosis of L and a group of 60 horses had a radiological diagnosis of NS. For each of the patients, the following details were noted: age, sex, breed, date of radiographic examination, radiographs, radiology report, and radiological diagnosis, including the severity of laminitis (mild, moderate, or severe) in group L feet. In the affected group L, 40 patients with examinations between 2018 and 2022, and in the control group NS, 60 patients with examinations between 2020 and 2021 met the criteria given above.

Radiographs

For the purpose of this study, Digital Imaging and Communications in Medicine (DICOM) files of radiographs were evaluated and measured using the software ImageJ (Version 1.53e, Wayne Rasband and contributors, the National Institutes for Health [NIH]) and JiveX (Version 5.5, Visus Health IT GmbH). The study was based on native radiographs of the left and right unshod forelimbs of horses. Digital radiographs in dorsoproximal-palmarodistal projection were selected and obtained either using an Oxspring block for the foot and the X-ray beam at 90° to the plate or with the foot weight-bearing on the plate and the X-ray beam angled at 65° to the plate (ie, High coronary view). Only sagittal radiographs showing the phalanx proximalis, the phalanx media and the phalanx distalis with the os sesamoidale distale overlapping neither the processus palmaris lateralis or medialis of the phalanx distalis were analyzed. Radiographs were considered unsuitable for measurements and were excluded from analysis if gas shadows, incomplete depiction of the hoof, or foreign material in the region of interest, that is, the distal phalanx were noted. To standardize results to the size of the horse, a reference distance was measured from the medial to the lateral fovea ligamentaria of the proximal phalanx. Radiographs where new bone formation or superimposition of foreign material precluded this were also excluded.

Data collection from radiographs using "Arteries Analyzer/ImageJ"

Using the ImageJ software, a freely available new plugin (https://github.com/reiservalentina/Arteries-Analyzer-ImageJ-Plugin) named "Arteries Analyzer/ImageJ" was developed. The plugin was programmed specifically for this research, to enable an automated, objective analysis **(Supplementary Figure S1)**. The aim of the "Arteries Analyzer" is to measure the osseous borders of the arterial channels[20,21] of the phalanx distalis from arcus terminalis to the margo solearis, and to characterize them numerically. The Plot Profile lists the precise

measurements of the arterial channels based on very limited manual input. As a pilot, this was tested and optimized several times by the authors using radiographs, that were not included in the main part of the study (eg, of horses where radiography had been carried out on a single forelimb only). The sequence of processing is as follows: After starting ImageJ the plugin Arteries Analyzer is found under the folder "Plugins" and the subfolder "Analyze." After launching the Arteries Analyzer the radiograph to analyze can be opened by ImageJ, and the software guides the user through every step of the measurements by showing pop-up icons. After scaling using a straight line **(Figure 1)** another straight line was drawn by the human evaluator between the lateral and the medial fovea ligamentaria of the phalanx proximalis ($b_{proximal\ pastern}$). To ensure comparability between horses, all data obtained from the arterial channels is given as a ratio of the width of the distal aspect of the proximal phalanx ($b_{proximal\ pastern}$). The next step for the human evaluator was to place a transversal (lateromedial) reference line (x) at the level of the coffin joint by connecting the most distal contours of the medial and lateral half of the joint surface within the distal phalanx. This line was used by the software to calculate the angle (β) in degrees (°) of the arterial channels measured. The angle was measured by the software between this line (x) and the midline (g). The midline (g) was defined by the software as the line described by the middle between the starting points of (d) and (e) as well as the middle between intersections of (f) with (d) and (e). By definition, angles were measured by the software starting from medial, so that the angle (β) measured < 90° if the artery was (dorso-)medial and > 90° if the artery was located (dorso-) lateral. The length of the artery g was afterward calculated by the software using

$$g = \frac{d + e}{2} \quad (1)$$

and the relative length of the artery was calculated by the software using the width of the proximal pastern:

$$g_{rel} = \frac{g}{(b_{proximal\ pastern})} \quad (2)$$

Further steps concern individual arteries. Of each individual artery, borders were drawn by the human evaluator counterclockwise, that is, starting on the medial side of the left fore distal phalanx and on the lateral side of the right fore distal phalanx. The first straight line measured as d and the second straight line as e starting from the visible end of the artery at the margo solearis toward the arcus terminalis. These lines were drawn by the evaluator as far as the borders of the artery were clearly discernible. The angle between the 2 lines (d) and (e) was described as the opening angle (α). In the next step, the closing line (f) of the visible artery was created by manually drawing a transversal straight line closing the artery at the point where the borders indicated by lines d and e ended proximally. After that, the Arteries Analyzer determined the surface A_A of

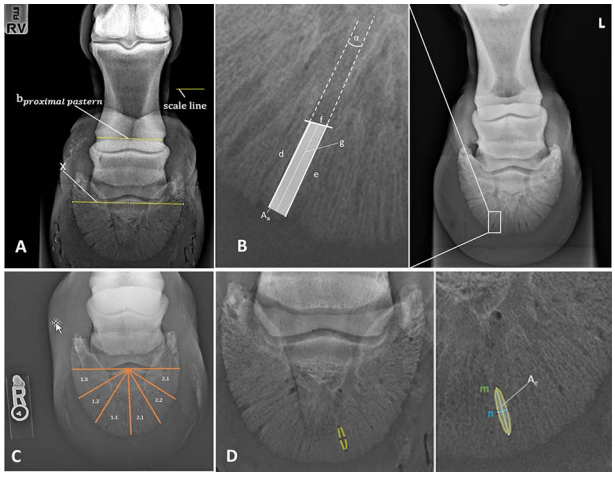

Figure 1—(A) Oxspring (0°; dorsoproximal–palmarodistal) radiographic view of a right forefoot of horse Nr. 9 without laminitis to illustrate the first measurements using the "Arteries Analyzer/ImageJ" a freely available new plugin of the ImageJ software used to establishing and validating an objective method of radiographic diagnosis of anatomic changes in laminitic feet of horses. The aim of the "Arteries Analyzer" is to measure the osseous margins/borders/surroundings of the arterial channels of the phalanx distalis from arcus terminalis to the margo solearis, and to characterize them numerically. Scale Line = line drawn manually using the line straight line function. b_(proximal pastern) = straight line drawn between the lateral and the medial fovea ligamentaria of the phalanx proximalis. To ensure comparability between horses of different size, all data obtained from the arteries is given as a ratio of the width of the distal aspect of the proximal phalanx (b_proximal pastern). x = reference line placed transversal (lateromedial) at the level of the coffin joint by connecting the most distal contours of the medial and lateral half of the joint surface within the distal phalanx. This line was used to calculate the angle (β) in degrees (°) of the arterial channels measured. (B) Oxspring (0°; dorsoproximal–palmarodistal) radiographic view of the left forefoot of horse Nr. 5 with laminitis to illustrate the measurements of a single Artery using the "Arteries Analyzer/ImageJ." d = first straight line drawn, starting counterclockwise from the visible end of the artery at the margo solearis towards the arcus terminalis. e = second line drawn, starting from the visible end of the artery at the margo solearis towards the arcus terminalis. f = e closing line (f), created by manually drawing a transversal straight line closing the artery at the point where the borders indicated by lines d and e ended proximally. g = the line described by the middle between the starting points of (d) and (e) as well as the middle between intersections of (f) with (d) and (e). A_A = surface of the artery. (C) Oxspring (0°; dorsoproximal–palmarodistal) radiographic view of the right forefoot of horse number 3 with laminitis to illustrate the measurements of ellipses. m = major axis, parallel to a line from the arcus terminalis to the margo solearis. n = minor axis parallel to the margo solearis. Area Ae = surface of the ellipse. (D) High coronary (65°; dorsoproximal–palmarodistal) radiographic view of a forefoot of horse number 6 laminitis to illustrate the subgroups. Those were established to categorize the localization of arteries and ellipses. With the first number indicating medial (1) or lateral (2) and the second number dorsal (1), dorsoabaxial (2), and abaxial (3) resulting in the categories 1.1, 1.2, 1.3, 2.1, 2.2, and 2.3.

the artery calculating the area of the created polygon using the formula:

$$A_{Arel} = \frac{A_A}{w^2} \quad (3)$$

The overall width (w) and the overall relative width (w_{rel}) of the artery were calculated by the software as follows:

$$w = \frac{A_A}{g} \quad (4)$$

$$w_{rel} = \frac{w}{b_{distal\ fetlock}} \quad (5)$$

All visible arterial channels were measured similarly. After the arteries, the analyzer prompted the assessment of ellipses to be analyzed. As a definition in the present paper, ellipses were similar to arterial channels but without reaching the visible margo solearis. Also, they were elliptical structures and wider and rounder than the arterial channels. Ellipses were outlined by the human evaluator counterclockwise similar to the arterial channels by placing and shaping an ellipse congruent to the radiolucency using the shapes selection of imageJ. The Arteries Analyzer then listed the measurements of this structure. The ellipses within the distal phalanx always have a major axis m parallel to a line from the arcus terminalis to the margo solearis and a minor axis (n) parallel to the margo solearis. After the program determined the area A_E of the ellipse the relative area of the ellipse was calculated as follows:

$$A_{Erel} = \frac{A_E}{b_{distal\ fetlock}^{\ 2}}. \quad (6)$$

All visible arterial channels and ellipses in the dorsal half of the distal phalanx were measured. Cases where no arterial channels were visible within the dorsal half of the distal phalanx (ie, dorsal to line x) were not used for analysis. To categorize the localization of arterial channels and ellipses 6 sectors were established by the human evaluator, with the first number indicating medial (1) or lateral (2) and the second number dorsal (1), dorso-abaxial (2), and abaxial (3) resulting in the categories 1.1, 1.2, 1.3, 2.1, 2.2, and 2.3.

Statistical analysis

The statistical data analysis was performed using the commercial software program IBM SPSS Statistics, version 28, IBM Corp. Due to the small sample size, statistical analysis was performed using nonparametric tests. Significance was set at $P < .05$. Comparisons between parameters of groups (L and NS), of left and right limbs, as well as of arterial channels of limbs with and without ellipses, and of arterial channels and ellipses in the different sectors of the distal phalanx were carried out using Wilcoxon and the Mann-Whitney *U* tests, respectively. Statistic correlations between parameters were calculated as Pearson Correlation coefficients (PCC). Median values, as well as maximum and minimum values, were used to present the results of the parameters obtained.

The reliability and repeatability of the software were tested using Friedmann test; furthermore, correlations between the results of the 3 evaluators and of the 5 evaluations were correlated using PCC. The repeatability of the measurements was tested on 10 radiographs (5 randomly selected radiographs of group NS and 5 randomly selected radiographs of group L) analyzed a total of 5 times by 3 evaluators (twice by 2 evaluators and once by the third evaluator). The following, are referred to as evaluation 1.a, 1.b, 2.a, 2.b, and 3.a representing the number of the evaluator (1, 2, and 3) as well as the measurement cycle (a, b) **(Supplementary Figures S2 and S3)**. A total of 374 structures (arteries and ellipses) were outlined and measured in this way.

Results

Horses

In group L, radiographs (left and right foot) of 45 horses were analyzed, and after the exclusion of horses, due to insufficient quality of the images or data only from 1 forelimb, data, and radiographs of 20 horses were used for this study. Out of the 60 horses available for possible inclusion in group NS, the first 20 with suitable radiographs were used for this study. A total of 3 ponies, 16 horses and 1 draft horse (mean age = 20 years) in group L and 3 ponies and 17 horses in group NS (mean age = 10 years) were selected.

Radiographs

Forty radiographs (20 left and 20 right; 14 Oxspring, 26 High coronary) of the forelimbs of 20 horses in group L and forty radiographs (20 left and 20 right; 40 Oxspring) of 20 horses in group NS met the selection criteria. The grade of laminitis in group L ranged from mild to severe with rotation of the distal phalanx ranging from 1.6 to 16.5°. On average laminitis was graded as mild radiographically with an average rotation of 6°. In the NS group the radiographically measured angle between the distal phalanx and the dorsal hoof wall was ranging from −3.5° to 4.0°, with an average angle of 0.02°. The distance from the medial to the lateral fovea of the first phalanx ranged from 55.4 to 79.6 mm and was on average 62.3 mm in group L and ranged from 53.0 to 68.1 mm and was on average 62.1 mm in group NS.

Comparison between left and right forelimbs

Parameters per limb and parameters of arterial channels and ellipses were compared between left (L) and right (R) forelimbs, with 22 parameters per limb showing no significant difference between sides, and 4 parameters showing significant differences. Compared with the right forelimb, left forelimb ellipses had a shorter minor axis (L median 6.9 mm, range = 3.9–14.7 mm; R median = 7.4 mm, range = 3.6–9.8 mm; $P = .022$), a smaller area (L median = 163.4 mm^2, range = 44.4–665.9 mm^2, R median = 180.4 mm^2, range = 56.2–304.7 mm^2; $P = .012$), and

Table 1—Parameters of arterial channels and ellipses in the distal phalanx identified on dorsoproximal-palmarodistal radiographs comparing laminitis (group L, 20 horses, 40 forelimbs) and navicular syndrome without any signs of laminitis (group NS, 20 horses, 40 forelimbs) based on clinical and diagnostic imaging record review.

Arteries/Ellipses	Group L (n = 40)					Group NS (n = 40)				
Limbs with A	40					40				
Number of A	164					187				
Mean number of A per limb (min-max)	4.1 (1-8)					4.6 (1-8)				
Limbs with E	32[a]					15[a]				
Number of E	90[b]					36[b]				
Mean number E per limb (min-max)	2.5 (0-5)					0.7 (0-5)				
Sctr.	**Angle β (°)**	**Rel area (%)**	**Rel length (%)**	**Rel width (%)**	**Opening angle α (°)**	**Angle β (°)**	**Rel area (%)**	**Rel length (%)**	**Rel width (%)**	**Opening angle α (°)**
All sctr.	86.4[c] (64.1-125.6)	0.65[d] (0.35 -1.21)	17.8[e] (11.7-28.0)	3.5 (2.6- 4.8)	2.8[f] (0.5- 6.5)	91.4[c] (75.9-123.7)	0.86[d] (0.51-1.73)	24.3[e] (16.7-36.6)	3.5 (2.7- 5.0)	2.7[f] (0.7- 4.8)
1.1 (L n = 24; NS n = 30)	68.9 (85.0-50.7)	0.5[g] (0.2-0.8)	17.3[h] (9.7-27.7)	3.1 (1.9-4.2)	1.9 (0.1- 8.6	71.7 (60-88)	0.6[g] (0.4-1.6)	21.2[h] (16.0-32.3)	3.2 (2.4-5.7)	1.9 (0.1- 6.4)
1.2 (L n = 40; NS n = 30)	42.9 (31.6-57.7)	0.8 (0.2-1.8)	48.[i] (17.9-110.3)	3.5 (2.1-5.8)	2.2[j] (0.1- 11.4)	42.8 (30.1-60.1)	0.8 (9.4-1.7)	53.9[i] (20.7-114.9)	3.5 (2.1-5.6)	1.6[j] (0.1- 10.8)
1.3 (L n = 16; NS n = 21)	17.4[k] (3.9-28.7)	0.7[l] (0.5-1.9)	20.4[m] (11.1-33.8)	3.9 (2.6-5.6)	2.4 (0.1- 7.3)	25.9[k] (12.3-29.7)	1.1[l] (0.5-1.8)	27.9[m] (18.9-45.1)	3.8 (3.6-25.1)	1.4 (0.1- 7.2)
2.1 (L n = 35; NS n = 37)	114.6[n] (99.4-129.3)	0.5[o] (0.3-1.1)	15.7[p] (11.6-24.7)	3.4 (2.3-4.4)	4.6[q] (0.1- 10.3)	109.3[n] (95.2-124.8)	0.6[o] (0.3-1.9)	20.3[p] (12.4-40.7)	3.2 (1.1-5.0)	1.7[q] (0.2- 5.4)
2.2 (n = 37/ n = 46)	142.6[r] (152.6-120.3)	0.6[s] (0.3-1.3)	17.3[t] (10.9-30.9)	3.6 (2.3- 5.6)	2.3 (0.0- 11.7)	133.9[r] (120.2-149.8)	0.7[s] (0.3-2.1)	22.7[t] (11.8-36.9)	3.3 (1.9-6.1)	1.5 (0.0- 11.9)
2.3 (n = 12/ n = 23)	159.4 (151.4-179.7)	0.8 (0.3-1.6)	21.2 (13.0-30.9)	4.2 (2.8-5.7)	2.3 (0.3- 8.6	160.2 (150.1-170.2)	1.2 (0.5-2.2)	28.5 (15.5-50.0)	3.8 (3.1-6.8)	1.3 (0.1-7.2)

Parameters (median, minimum, and maximum values) of the arterial channels per limb and per sector (1.1-2.3) within the distal phalanx as defined in Figure 1 are listed. Values with the same superscript differ significantly. A = Arterial channel. E = Ellipse. Sctr. = Sectors. L = Group L. NS = Group NS. Rel = Relative to proximal pastern.

[a]$P < .01$, [b]$P < .01$, [c]$P = .014$, [d]$P < .00$, [e]$P < .00$, [f]$P = .028$, [g]$P = .002$, [h]$P < .001$, [i]$P = .011$, [j]$P = .018$, [k]$P = .003$, [l]$P = .015$, [m]$P = .007$, [n]$P = .039$, [o]$P = .004$, [p]$P < .001$, [q]$P = .007$, [r]$P = .021$, [s]$P = .015$, [t]$P < .001$.

a smaller relative area (L median 0.29%, range = 0.13–0.64%, R median = 0.35%, range = 0.22–0.57%; *P* = .039). Furthermore, the localizations of the ellipses within the distal phalanges were significantly different, with the left forelimbs showing ellipses slightly more abaxial than the right forelimbs (*P* = .023). Parameters of arterial channels and of ellipses showed no significant differences between right and left forelimbs. Due to the majority of parameters being side-independent, further analysis was carried out without considering the body side.

Analysis per limb

Arterial channels did not differ significantly between groups **(Table 1)** but the number of ellipses per limb differed significantly between the 2 groups (L and NS), with 32 limbs in group L showing ellipses compared with 15 in group NS, and radiographs in group L showing significantly more ellipses than those of the control group NS **(Table 2)**. A significant positive correlation was determined between the number of ellipses per limb and the measured degree of rotation of the distal phalanx (PCC 0.392; *P* < .01, n = 80) as well as with the radiologically evaluated severity of laminitis (PCC 0.495; *P* < .01, n = 80). Additionally, parameters of arterial channels in limbs with and without ellipses were compared independent of group (L or NS) **(Table 3)**. In the limbs where ellipses were present, the number of arterial channels and ellipses per limb was negatively correlated, with more ellipses present in radiographs with fewer arterial channels **(Figure 2)**.

Reliability and repeatability tests

There was a very high consistency of identifying structures as either arteries or ellipses within the measurements. Only 7 structures of the 374 structures were classified as arteries in 1–4 evaluations and as ellipses in the remaining 1–4 evaluations. In these cases, the artery measurements (relative area, relative length, and relative width) were tested against the ellipse measurements representing similar dimensions (relative area, relative main axis, and relative minor axis), and no significant differences were found (relative area artery vs relative area ellipse *P* = .76; relative length artery vs relative main axis ellipse *P* = .54; relative width artery vs relative minor axis ellipse *P* = .76).

In the interpersonal comparisons, only 4 out of 80 tests (3 evaluations by 3 different evaluators, with 10 parameters each) showed significant differences (relative area 1.a vs. 2.b, *P* = .02; relative major axis 1.a vs 2.b, *P* = .00; relative length 1.a vs 2.b, *P* = .00; relative length 1.a vs 3.a, *P* = .02). For intrapersonal comparison measurements showed high consistency. Only 1 out of 20 tests showed a significant

Table 2—Median and range values of the measurements of the ellipses of the radiographs without laminitis (NS) and with diagnosed laminitis (L) and parameters of the ellipses (medians and ranges) in the different sectors (1.1, 1.2, 2.1, and 2.2).

Group L	All limbs with E (n = 32)	L sctr. 1.1 (n = 40)	L sctr. 1.2 (n = 12)	L sctr. 1.3 (n = 0)	L sctr. 2.1 (n = 26)	L sctr. 2.2 (n = 12)	L sctr. 2.3 (n = 0)
Rel. main axis (%)	13.0 (6.7-21.8)	12.7 (6.7-25.1)	13.6 (8.1-20.1)	—	12.9 (9.1-20.6)	13.1 (9.7-18.3)	—
Rel. minor axis (%)	3.1 (2.0-4.3)	2.8 (1.3-4.7)	2.8 (2.5-4.3)	—	3.4 (1.9-5.0)	2.8 (2.2-6.3)	—
Rel. area (%)	0.3 (0.1–0.6)	0.2 (0.1-0.7)	0.3 (0.2-0.6)	—	0.4 (0.2-0.8)	0.3 (0.2-0.6)	—
Group NS	**All limbs with E n = 15)**	**NS sctr. 11 (n = 19)**	**NS sctr. 12 (n = 7)**	**NS sctr. 13 (n = 0)**	**NS sctr. 21 (n = 10)**	**NS sctr. 22 (n = 0)**	**NS sctr. 23 (n = 0)**
Rel. main axis (%)	14.2 (6.8-17.6)	14.9 (6.8-22.3)	13.4 (5.5-17.1)	—	12.6 (7.2-19.8)	—	—
Rel. minor axis (%)	3.2 (2.2-4.8)	3.1 (2.2-4.4)	3.2 (2.5-4.9)	—	2.7 (1.8-5.2)	—	—
Rel. area (%)	0.3 (0.2-0.6)	0.3 (0.2-0.66)	0.3 (0.1-0.6)	—	0.33 (0.1-0.4)	—	—

The sectors are defined in Figure 4. No ellipses were detected in sector 1.3 and sector 2.3. No significant differences were found between the ellipses of group L and of group NS. See Table 1 for Key.

Table 3—Medians and ranges of measurements of arterial channels in forelimb distal phalanx radiographs horses with laminitis (L) and without laminitis (NS) with ellipses and without ellipses.

Limbs	Angle (β)(°)	Rel. area (%)	Rel. length (%)	Rel. width (%)	Opening angle α (°)
Limbs with E (n = 47, group L n = 32, group NS n = 15)	104.9[a] (3.9-179.9)	0.700[b] (0.23-2.27)	20.6[c] (8.2-50.1)	3.4[d] (1.9-6.8)	1.9 (0.01-11.9)
Limbs without E (n = 33, group L n = 8, group NS n = 25)	110.9[a] (3.9-179.9)	0.698[b] (0.23-2.27)	21.1[c] (9.7-50.1)	3.3[d] (1.9-6.8)	1.9 (0.02-11.9)

Values with the same superscript are significantly different. See Table 1 for Key.
[a]*P* = .000, [b]*P* = .001, [c]*P* = .002, [d]*P* = .034.

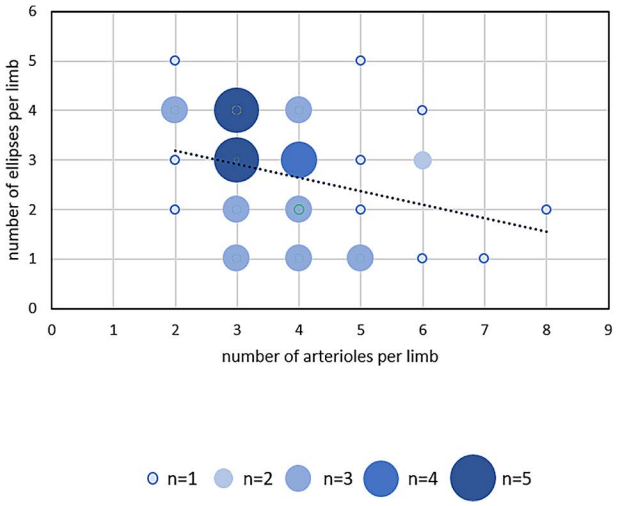

Figure 2—Scatterplot and linear trendline of the number of ellipses vs the number of arteries per limb in all 47 limbs with ellipses (PCC −0.181; *P* = 0.224, N = 47).

difference (number of arteries 2.a vs. 2.b, *P* = .03). Correlating the mean results of each parameter per limb of all 5 evaluations, irrespective of the individual artery or ellipse measured there was a mean correlation of 0.39 (Pearson Correlation Coefficient), with a significance of 0.29 from n = 8.93.

Individual arteries and ellipses showed no significant differences in interpersonal and intrapersonal comparisons, with a mean *P*-value of .73. This underlines a high repeatability between evaluators and measurement cycles. All correlations between the same arteries and the same ellipses were calculated between the 5 measurements of the 3 evaluators, the Pearson Correlation Coefficient of the arteries was 0.63; with a significance of 0.09 from mean n = 37, and the mean Pearson Correlation Coefficient of the ellipses was 0.40, with a significance of 0.2 from a mean n = 17.6.

Mean relative difference between the software output and the values measured without the use of the new plugin was 4.1% for relative artery area, 1.2% for relative artery length, 4.3% for relative artery width, 9.2% for the artery opening angle, and 1.9% for the artery angle. Regarding the ellipses, mean relative difference was 4.9% for ellipse relative major axis, 4.2% for ellipse relative minor axis, and 5.9% for ellipse relative area. No significant differences between the human and plugin measurements of the same structures were found, this is additionally shown by the significant correlations of human and plugin measurements (PCC 0.97; *P* < .01, n = 26).

Discussion

For this study, we examined dorsoproximal-palmarodistal radiographs of the distal phalanx of equine forelimbs as these projections provide the clearest image of the quality of the distal phalanx and of the terminal arch and its branches.[13,22] Although these projections are not routinely obtained for the evaluation of horses with laminitis, they highlight the solear margin of the distal phalanx where bone remodeling or lysis commonly occurs.[11] Depending on the suspected condition or specific diagnostic question, clinicians select either "high coronary" projections or Oxspring projections, as these projections differ by 25° in the angulation of the radiographic beam onto the plate. Both of these projections have been used[11,13,23] to describe changes of the hoof wall and of the distal phalanx, such as increased thickness of the stratum internum-corium tissues with lamellar wedge formation[24] or to highlight the solear margin of the distal phalanx which aids lesion identification in this area.[25] As radiographs used in the present study were analyzed retrospectively, either Oxspring or high coronary projections were available for individual horses. The physiological angle of the dorsal wall of front feet in horses is described to have angles between 45 and 50[26,27]and it is reported with a mean angle of around 50.[28,29] In horses without laminitis, this is representative of the angle of the dorsal contour of the distal phalanx. However, in laminitic feet after rotation of the distal phalanx, the angle of the dorsal contour of the distal phalanx is more upright, and high coronary projections allow a more detailed depiction of the margo solearis of the distal phalanx. Additionally, the trimming of heels and dorsal hoof wall are major influences on the angle of the distal phalanx in relation to the radiographic plate. Therefore, differences in angle between the distal phalanx and the radiography plate would also have been present if only 1 of the 2 dorsoproximal-palmarodistal projections had been used.

Similar to the study population of previous studies on laminitis[24,30–33] where foals and young horses were not included in the examination, this was also the case in the present study as laminitis is rarely seen in young horses. Even though the growth plates in the digits are the first to close between 8.1 to 8.5 months of age, the majority of growth plates are only fully closed at the age of approximately 3 years.[34] The development periods of horses also is completed very early in life, generally by 2 years of age, the horse enters skeletal maturity achieving most measures of maturity used within the human literature, including the plateauing of vertical height, closure of growth plates, and adult ratios of back length:wither height and limb length:wither height.[35] To enhance the comparative value of the radiographic measurements obtained in the present study, the minimum age selected was 4 years.

The increased blood flow to the digit in horses suffering from laminitis is an early clinical finding, picked up during clinical examination as increased, bounding digital pulsation. With prolonged increased blood flow bony changes of the arterial channels due to the pressure of the bounding pulse wave were expected. A similar development is seen in human patients, where radiological evidence of nutrient canals beyond mandibular anterior tooth root apices is associated with hypertension.[36] Before starting the analysis, we expected arterial channels to be wider in group L than in group NS, based on the presumptive

higher blood pressure[3] in these arteries[23] forcing the adjacent bone to recede. However, the width of the arterial channels was similar in the 2 groups. The arterial channels in the healthy distal phalanges were longer and had a larger area, which is another measure of the fact that during the process of laminitis, the third phalanx recedes.[37] However, the larger opening angle of the arterial channels could be a result of the changes in the systolic blood pressure[3] possibly combined with reduced bone density at the margo solearis during laminitis.[24]

The presence of ellipses in more than 3/4 of laminitic distal phalangeal radiographs but only in less than half of healthy distal phalangeal radiographs was a striking difference.

The shape of the ellipses with their main axis similar to the arterial channels along straight lines from the arcus terminalis to the margo solearis, makes it likely that they represent vascular structures. Also, ellipses are seen in similar positions to arterial channels. The fact that there were fewer arterial channels but more ellipses in the distal phalanges of horses suffering from laminitis suggests a development from a healthy artery to a laminitic artery and then onto an ellipse. The negative correlation between ellipses and arterial channels, in distal phalanges where ellipses were found, underlines the development of healthy arterial channels into "disease ellipses" in horses with laminitis. Thus presence and number of ellipses in the distal phalanx appear to indicate bone change, as there is a significant, positive correlation between the evaluated severity of laminitis and the measured degree of rotation of the distal phalanx within the hoof capsule. No significant differences were found in the shape and size of the ellipses between the 2 groups (L and NS) and, therefore, relevance of these features remains questionable.

If arterial channels develop into ellipses, additional arterial channels have to become visible in the laminitic distal phalanges, as the sum of arterial channels and ellipses in the sectors of group L exceeds the sum in the sectors of group NS. Such a development may be due to the hypertension within bone of potentially reduced quality such as described in the vascular canals of the root of the teeth.[36] Due to the increased blood flow in laminitis, with localized/regional hypertension,[3] we expected the presence of more vascular structures in group L than in group NS, which is true, if the sum of ellipses and arterial channels is considered. However, the distribution of the sum of vascular structures is markedly different, with the number of arterial channels smaller in L than in NS distal phalanges but the higher number of ellipses more than outweighs this.

Analyses of the arterial channels and ellipses in the 6 sectors also showed no differences in the main parameters. An interesting finding was the absence of ellipses in sector 2.2 in group NS and the total absence in sector 2.3 regardless of group. The absence of ellipses in the lateral and abaxial part of the third phalanx could be explained by the smaller biomechanical stress in the third phalanx laterally than medially.[38,39] The increased biomechanical pressure on the medial side appears to induce the formation of ellipses. This theory is supported by the higher number of ellipses on the medial than on the lateral side (Table 2).

In many imaging studies in human medicine[40–42] software supported diagnosis and interpretation is widespread, and increasing. This is not yet similarly advanced in veterinary imaging, and the software tool used in the present study, that is, the Arteries Analyzer plugin of ImageJ, was developed to aid in the interpretation of radiographs in a clinical setting, but it is not a fully autonomous diagnostic tool. The measurement system can be classified as a composite human evaluator/software measurement, with the human evaluator identifying the structures and then applying the software to the structures already identified. The plugin allows quick and reliable measurements for comparisons of anatomic features of the development and severity of laminitis-associated bone changes. The repeatability and reliability of software-assisted measurements are now fully recognized in veterinary radiology,[43] and the results of the respective testing in the present study show adequate repeatability, better in arteries than in ellipses. This may also be the reason why the presence of ellipses, but not the measurements of ellipses were significantly different between L and NS distal phalanges. The influence of the handedness of the evaluators when outlining the structures cannot be ruled out, and, as the 3 evaluators were righthanded, this could not be assessed in the present study.

The present study represents the first occasion in which a specifically developed software tool was applied for the refined evaluation of distal phalanx radiographs of horses with laminitis. Specifically, the results of the present study have indicated that this tool may be used to successfully develop a robust means of identifying anatomic changes in equine laminitic feet from Oxspring or high coronary radiographic projections. This represents a logical progression to former methods of objective radiographic assessment[33] providing the basis for widening the subjective radiological assessments.

With this study, the goal of creating a new measurement tool for the analysis of structures outlined by a human evaluator in horses with laminitis was achieved. With little additional effort on either of the 2 dorsoproximal palmarodistal radiographic view images it may be possible to add a helpful new diagnostic and radiological tool to evaluate cases of laminitis even more reliably.

Acknowledgments

None reported.

Disclosures

The authors have nothing to disclose. No AI-assisted technologies were used in the generation of this manuscript.

Funding

The authors have nothing to disclose.

References

1. Mitchell CF, Fugler LA, Eades SC. The management of equine acute laminitis. *Vet Med (Auckl).* 2015;6:39–47.
2. Peroni JF, Moore JN, Noschka E, et al. Predisposition for venoconstriction in the equine laminar dermis: implications in equine laminitis. *J Appl Physiol (1985).* 2006;100(3):759–763. doi:10.1152/japplphysiol.00794.2005
3. Morgan RA, Keen JA, Walker BR, et al. Vascular dysfunction in horses with endocrinopathic laminitis. *PLoS ONE.* 2016;11(9):e0163815. doi:10.1371/journal.pone.0163815
4. Pollitt CC, Visser MB. Carbohydrate alimentary overload laminitis. *Vet Clin North Am Equine Pract.* 2010;26(1):65–78. doi:10.1016/j.cveq.2010.01.006
5. Hood DM, Grosenbaugh DA, Mostafa MB, et al. The role of vascular mechanisms in the development of acute equine laminitis. *J Vet Intern Med.* 1993;7(4):228–234. doi:10.1111/j.1939-1676.1993.tb01012.x
6. Johnson PJ, Messer NT, Slight SH, et al. Endocrinopathic laminitis in the horse. *Clin Tech Equine Pract.* 2004;3(1):45–56. doi:10.1053/j.ctep.2004.07.004
7. Ingle-Fehr JE, Baxter GM. Evaluation of digital and laminar blood flow in horses given a low dose of endotoxin. *Am J Vet Res.* 1998;59(2):192–196.
8. Hinckley KA, Fearn S, Howard BR, et al. Nitric oxide donors as treatment for grass induced acute laminitis in ponies. *Equine Vet J.* 1996;28(1):17–28. doi:10.1111/j.2042-3306.1996.tb01586.x
9. Schneider DA, Parks AH, Eades SC, et al. Palmar digital vessel relaxation in healthy horses and in horses given carbohydrate. *Am J Vet Res.* 1999;60(2):233–239.
10. Pollitt CC. Equine laminitis. *Clin Tech Equine Pract.* 2004;3(1):34–44. doi:10.1053/j.ctep.2004.07.003
11. Herthel D, Hood DM. Clinical presentation, diagnosis, and prognosis of chronic laminitis. *Vet Clin North Am Equine Pract.* 1999;15(2):375–94. doi:10.1016/S0749-0739(17)30151-7
12. Parks A, O'Grady SE. Chronic laminitis: current treatment strategies. *Vet Clin North Am Equine Pract.* 2003;19(2):393–416. doi:10.1016/S0749-0739(03)00019-1
13. Rosenstein DS, Bowker RM, Bartlett PC. Digital angiography of the feet of horses. *Am J Vet Res.* 2000;61(3):255–259. doi:10.2460/ajvr.2000.61.255
14. Rucker A. Equine venography and its clinical application in North America. *Vet Clin North Am Equine Pract.* 2010;26(1):167–177. doi:10.1016/j.cveq.2009.12.008
15. Dyson S, Murray R, Schramme M, et al. Magnetic resonance imaging of the equine foot: 15 horses. *Equine Vet J.* 2003;35(1):18–26. doi:10.2746/042516403775467531
16. Wongaumnuaykul S, Siedler C, Schobesberger H, et al. Doppler sonographic evaluation of the digital blood flow in horses with laminitis or septic pododermatitis. *Vet Radiol Ultrasound.* 2006;47(2):199–205. doi:10.1111/j.1740-8261.2006.00128.x
17. Dyson S, Murray R. Verification of scintigraphic imaging for injury diagnosis in 264 horses with foot pain. *Equine Vet J.* 2007;39(4):350–355. doi:10.2746/042516407X185430
18. Ackerman N, Garner HE, Coffman JR, et al. Angiographic appearance of the normal equine foot and alterations in chronic laminitis. *J Am Vet Med Assoc.* 1975;166(1):58–62.
19. Aguirre CN, Talavera J, Del Fernández Palacio MJ. Usefulness of Doppler ultrasonography to assess digital vascular dynamics in horses with systemic inflammatory response syndrome or laminitis. *J Am Vet Med Assoc.* 2013;243(12):1756–1761. doi:10.2460/javma.243.12.1756
20. Schade SM, Arnoczky SP, Bowker RM. The microvasculature in the equine distal phalanx: implications for fracture healing. *Vet Comp Orthop Traumatol.* 2014;27(2):102–106. doi:10.3415/VCOT-13-08-0105
21. Jennings R, Premanandan C. *Veterinary histology.* The Ohio State University, 2017.
22. Whitlock J, Dixon J, Sherlock C, et al. Technical innovation changes standard radiographic protocols in veterinary medicine: is it necessary to obtain two dorsoproximal-palmarodistal oblique views of the equine foot when using computerised radiography systems? *Vet Rec.* 2016;178(21):531. doi:10.1136/vr.103396
23. Trout DR, Hornof WJ, Linford RL, et al. Scintigraphic evaluation of digital circulation during the developmental and acute phases of equine laminitis. *Equine Vet J.* 1990;22(6):416–421. doi:10.1111/j.2042-3306.1990.tb04308.x
24. Engiles JB, Galantino-Homer HL, Boston R, et al. Osteopathology in the equine distal phalanx associated with the development and progression of laminitis. *Vet Pathol.* 2015;52(5):928–944. doi:10.1177/0300985815588604
25. Sherlock C, Parks A. Radiographic and radiological assessment of laminitis. *Equine Vet Educ.* 2013;25(10):524–535. doi:10.1111/eve.12065
26. Nauwelaerts S, Hobbs SJ, Back W. A horse's locomotor signature: COP path determined by the individual limb. *PLoS ONE.* 2017;12(2):e0167477. doi:10.1371/journal.pone.0167477
27. Hertsch B, Hoppner S, Dallmer H. *The hoof and how to protect it without nails.* 1st ed. First Salzhausen-Putensen, 1996.
28. Clayton HM, Gray S, Kaiser LJ, et al. Effects of barefoot trimming on hoof morphology. *Aust Vet J.* 2011;89(8):305–311. doi:10.1111/j.1751-0813.2011.00806.x
29. Oosterlinck M, Pille F, Back W, et al. A pressure plate study on fore and hindlimb loading and the association with hoof contact area in sound ponies at the walk and trot. *Vet J.* 2011;190(1):71–76. doi:10.1016/j.tvjl.2010.08.016
30. Arble JB, Mattoon JS, Drost WT, et al. Magnetic resonance imaging of the initial active stage of equine laminitis at 4.7 T. *Vet Radiol Ultrasound.* 2009;50(1):3–12. doi:10.1111/j.1740-8261.2008.01483.x
31. de Laat MA, van Eps AW, McGowan CM, et al. Equine laminitis: comparative histopathology 48 hours after experimental induction with insulin or alimentary oligofructose in standardbred horses. *J Comp Pathol.* 2011;145(4):399–409. doi:10.1016/j.jcpa.2011.02.001
32. Faleiros RR, Johnson PJ, Nuovo GJ, et al. Laminar leukocyte accumulation in horses with carbohydrate overload-induced laminitis. *J Vet Intern Med.* 2011;25(1):107–115. doi:10.1111/j.1939-1676.2010.0650.x
33. Cripps PJ, Eustace RA. Radiological measurements from the feet of normal horses with relevance to laminitis. *Equine Vet J.* 1999;31(5):427–432. doi:10.1111/j.2042-3306.1999.tb03844.x
34. Strand E, Braathen LC, Hellsten MC, et al. Radiographic closure time of appendicular growth plates in the Icelandic horse. *Acta Vet Scand.* 2007;49(1):19. doi:10.1186/1751-0147-49-19
35. Rogers CW, Gee EK, Dittmer KE. Growth and bone development in the horse: when is a horse skeletally mature? *Animals (Basel).* 2021;11(12). doi:10.3390/ani11123402
36. Hasan S, Jahan U, Saeed S, et al. Prevalence of nutrient canals in mandibular anterior intra-oral periapical radiographs (IOPARS) in patients with chronic systemic diseases - a cross-sectional study. *J Med Life.* 2022;15(5):661–668. doi:10.25122/jml-2022-0009
37. Engiles JB. Pathology of the distal phalanx in equine laminitis: more than just skin deep. *Vet Clin North Am Equine Pract.* 2010;26(1):155–165. doi:10.1016/j.cveq.2009.12.001
38. Rayfield EJ. Finite element analysis and understanding the biomechanics and evolution of living and fossil organisms. *Annu Rev Earth Planet Sci.* 2007;35(1):541–576. doi:10.1146/annurev.earth.35.031306.140104
39. Newlyn HA, Collins SN, Cope BC, et al. Finite element analysis of static loading in donkey hoof wall. *Equine Vet J Suppl.* 1998;30(26):103–110. doi:10.1111/j.2042-3306.1998.tb05128.x

40. Heindel W, Weigel S, Gerß J, et al. Digital breast tomosynthesis plus synthesised mammography versus digital screening mammography for the detection of invasive breast cancer (TOSYMA): a multicentre, open-label, randomised, controlled, superiority trial. *Lancet Oncol.* 2022;23(5):601–611. doi:10.1016/S1470-2045(22)00194-2
41. Wahadat AR, Tanis W, Scholtens AM, et al. Normal imaging findings after aortic valve implantation on 18F-Fluorodeoxyglucose positron emission tomography with computed tomography. *J Nucl Cardiol.* 2021;28(5):2258–2268. doi:10.1007/s12350-019-02025-y
42. Waheed S, Tahir MJ, Ullah I, et al. The impact of dependence on advanced imaging techniques on the current radiology practice. *Ann Med Surg (Lond).* 2022;78:103708.10.1016/j.amsu.2022.103708
43. Park KM, Marcellin-Little DJ, Garcia TC. Evaluation of computer-aided design software methods for assessment of the three-dimensional geometry of the canine radius. *Am J Vet Res.* 2021;82(6):435–448. doi:10.2460/ajvr.82.6.435

Supplementary Materials

Supplementary materials are posted online at the journal website: avmajournals.avma.org.